Reactive Flow in Silicon Electrodes Assisted by the Insertion of Lithium

8 AUTHORS, INCLUDING:

Georgios A. Tritsaris
Harvard University
16 PUBLICATIONS **686** CITATIONS

SEE PROFILE

Zhigang Suo
Harvard University
348 PUBLICATIONS **16,542** CITATIONS

SEE PROFILE

Efthimios Kaxiras
Harvard University
418 PUBLICATIONS **15,250** CITATIONS

SEE PROFILE

Reactive Flow in Silicon Electrodes Assisted by the Insertion of Lithium

Kejie Zhao,[†] Georgios A. Tritsaris,[†] Matt Pharr,[†] Wei L. Wang,[‡] Onyekwelu Okeke,[‡] Zhigang Suo,[†] Joost J. Vlassak,[†] and Efthimios Kaxiras*,[†,‡]

[†]School of Engineering and Applied Sciences, Harvard University, Cambridge, Massachusetts 02138, United States
[‡]Department of Physics, Harvard University, Cambridge, Massachusetts 02138, United States

S Supporting Information

ABSTRACT: In the search for high-energy density materials for Li-ion batteries, silicon has emerged as a promising candidate for anodes due to its ability to absorb a large number of Li atoms. Lithiation of Si leads to large deformation and concurrent changes in its mechanical properties, from a brittle material in its pure form to a material that can sustain large inelastic deformation in the lithiated form. These remarkable changes in behavior pose a challenge to theoretical treatment of the material properties. Here, we provide a detailed picture of the origin of changes in the mechanical properties, based on first-principles calculations of the atomic-scale structural and electronic properties in a model amorphous silicon (a-Si) structure. We regard the reactive flow of lithiated silicon as a nonequilibrium process consisting of concurrent Li insertion driven by unbalanced chemical potential and flow driven by deviatoric stress. The reaction enables the material to flow at a lower level of stress. Our theoretical model is in excellent *quantitative* agreement with experimental measurements of lithiation-induced stress on a Si thin film.

KEYWORDS: Li-ion battery, silicon, first-principles, reactive flow
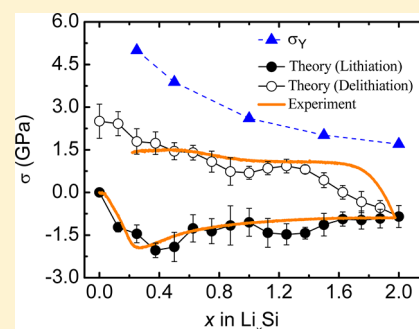
In the quest to develop high-energy density Li-ion batteries, materials that can absorb large amounts of Li are of great interest. Silicon shows a remarkable ability to absorb Li, making it a very promising anode material.[1] This, however, comes at the cost of very large deformation of the Si structure upon lithiation and a concurrent drastic change in mechanical properties, from the brittle nature of pure crystalline Si to an amorphous material that can undergo flow in the lithiated form.[2,3] This behavior is typical during the electrochemical cycling of high-capacity electrodes, such as lithium alloy anodes,[4] conversion oxides,[5] and sulfur cathodes,[6] all of which exhibit significant structural transformations and property changes induced by the Li insertion reaction.

The large amount of absorption of Li by Si results in a large volumetric expansion and severe structural changes. The lithiation-induced stress and fracture often lead to the loss of active materials and rapid decay of capacity, which limit its commercialization.[7] This mode of failure can be mitigated by manipulating the structural optimization and deformation patterns of nanostructured Si anodes. Examples include nanowires,[8] thin films,[9−11] hollow nanoparticles,[12] carbon−silicon composites,[13,14] and coated-hollow structures.[15−17] Recent experiments and theories show evidence that the large deformation of lithiated silicon can be accommodated by inelastic flow, which may avert fracture of nanostructured silicon.[18−23] To develop feasible nanostructured anodes, it is crucial to understand the lithiation, deformation, and stresses from a fundamental perspective.

Since the chemical interaction between Li and Si is local, first-principles quantum mechanical calculations can capture the microscopic mechanism of the lithiation reaction. The local chemical effects lead to the macroscopic mechanical behavior, such as flow of lithiated silicon. Lithiation and flow are both nonequilibrium processes. We extend the continuum theory of plasticity and formulate a yield condition by placing driving forces for lithiation and flow on the same footing. *In situ* experimental measurements of the stress evolution in an a-Si thin film during a lithiation and delithiation cycle serve both as the motivation for the theoretical work as well as a detailed quantitative test of the theory.

Previous atomistic studies include examining the energetics of Li in bulk crystalline silicon and silicon nanowires,[24−30] characterizing the elastic properties of the bulk,[31] and reproducing the volumetric and electric potential responses during lithiation and delithiation.[32−34] First-principles calculations have also been employed to illustrate the deformation mechanism of plasticity in lithiated silicon.[35] Here we present atomistic studies on the concurrent process of Li insertion and flow of amorphous lithiated silicon. Both the atomic insertion driven by the chemomechanical load and flow driven by the mechanical load contribute to the reactive flow of lithiated

silicon. We propose a yield function to describe the inelastic behavior. We correlate structural changes at the atomic scale with the macroscopic response and study the transition of electronic properties of Si upon Li insertion, from the semiconductor state to the metallic state.

We begin with a description of the experimental results that motivated this study. We measure the stress evolution in an a-Si thin film electrode during the first lithiation and delithiation cycle by the wafer curvature method. The solid electrolyte interface (SEI) layer might affect the stress measurement; such an effect has not been characterized at this writing. Li insertion and extraction result in a state of biaxial stress in the a-Si thin film deposited on a thick substrate. The thin film exerts forces on the substrate that result in elastic bending of the substrate. The average stress in the film can be deduced from the curvature of the substrate using Stoney's equation.[36] The electrochemical measurements are carried out in a custom three-electrode beaker cell, as illustrated in Figure 1s (Supporting Information). *In situ* stress measurements are performed with a multibeam optical sensor (MOSS). We describe the details of fabrication of amorphous silicon thin film electrodes, assembly of electrochemical cells, electrochemical measurements, and stress measurements in the Experimental Section. Similar experimental setups have been reported by other groups.[18,37,38]

The evolution of the biaxial stress in the a-Si thin film is shown in Figure 1. During the initial lithiation, the compressive
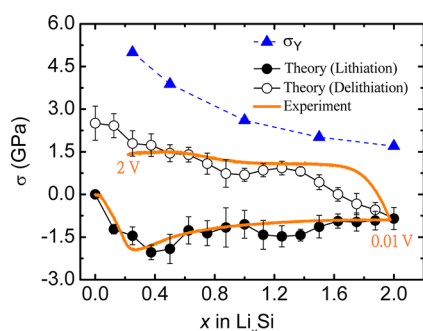
Figure 1. Evolution of the biaxial stress in an a-Si thin film electrode during a lithiation and delithiation cycle: The orange line shows the *in situ* measurement of the biaxial stress in the first lithiation cycle by the wafer curvature method. The electrode is cycled at 1C rate between 2 and 0.01 V vs Li/Li$^+$. The black lines with symbols (filled for lithiation, open for delithiation) show the evolution of the biaxial stress in an a-Si thin film electrode during a lithiation and delithiation cycle based on first-principles calculations. The error bars represent standard deviations obtained from several configurations at each Li concentration. The yield strength of lithiated Si at a given Li concentration, obtained by uniaxial tension simulations, is shown by triangles (the dashed line connecting the triangles is a guide to the eye).

stress increases linearly in the first stage, indicating an elastic response. The stress reaches an elastic limit of ~2 GPa for Li$_{0.25}$Si. We note that the elastic limit is higher than that reported in a previous study,[18] which may be due to neglecting the effect of the refractive index difference between the electrolyte and air in the previous study. With further lithiation, inelastic flow sets in to accommodate the additional volume expansion. The compressive flow stress decreases, reaching a value of ~1 GPa for Li$_2$Si at the cutoff potential 0.01 V vs Li/Li$^+$. The low lithiation capacity might be due to the fast charging rate (1C) in the experiment. Upon delithiation, the

unloading is initially elastic within a narrow range of Li composition. The stress reaches ~1 GPa in tension due to the plasticity of lithiated silicon. The flow stress increases slightly with further delithiation, reaching a value of ~1.5 GPa at the cutoff potential 2 V. The delithiation capacity is lower than that during lithiation; the irreversible capacity is often attributed to the formation of SEI.[1]

We simulate the stress evolution in an a-Si thin film electrode subject to a lithiation and delithiation cycle by employing first-principles computational methods. Such simulations allow a close inspection of the microscopic mechanism of lithiation and the associated deformation behavior. The first-principles calculations based on density functional theory (DFT) were performed using the SIESTA code.[39] The amorphous structure contains 64 Si atoms with periodic boundary conditions. This choice of supercell is consciously relatively small, because we are interested in exploring a large number of possible configurations of Si structures with various Li concentrations. Our choice of supercell affords such studies at a reasonable balance of computational cost and accuracy. The atomic structures, system energy, and mechanical stresses are calculated using a local-basis set of double-ς polarized atomic orbitals with an energy cutoff of 70 Ry (~952 eV). In energy optimization calculations, both the atomic coordinates and the supercell shape were fully relaxed. The energy optimization was considered complete when the magnitude of the force on each atom was smaller than 0.04 eV Å^{-1}.

The a-Si structure employed here was generated by quenching the liquid phase with explicit molecular dynamics using the environment dependent interatomic potential (EDIP) for Si,[40] as described in more detail in our previous work.[35,41] To simulate the behavior of the a-Si thin film bonded to a thick substrate, we constrain the in-plane deformation of the unit cell, with the lithiation-induced volume change accommodated by out-of-plane expansion (z-direction) of the unit cell. Kinetic effects, such as the long-range process of Li diffusion in Si, were considered in a separate calculation of the relevant energy barriers. We found that the lowest energy barrier for a single Li atom diffusion in the a-Si network is around 0.4 eV, significantly lower than that in the c-Si lattice (0.55 eV).[24,35] We also note that a typical value of lithium diffusivity in amorphous silicon is ~10^{-16} m^2 s^{-1};[42,43] the diffusion time for lithium through a 100 nm silicon film can be estimated as on the order of 100 s ($t \sim L^2/D$). Such time is much shorter than the charging time of a lithiation cycle at 1C. Thus, in the modeling of stress, we assume that diffusion is fast enough to allow for a uniform distribution of Li. A more detailed study of Li diffusion kinetics will be reported elsewhere.

At each Li concentration, we place Li atoms at energetically favorable positions in the a-Si network. To simulate an a-Si thin film, we constrain the deformation in the in-plane directions (x-, y-directions) and apply an incremental stretch to the z-direction with energy minimization at each step of the stretch. The structure resulting from energy minimization corresponds to the zero stress state in the z-direction. In order to eliminate the large variations in the calculation of in-plane stresses, we considered five possible configurations of lithiated silicon at a given Li concentration with different distributions of Li in each. We first identified 32 unique lowest-energy positions for a Li atom insertion into the a-Si network.[35] When the Li content is below Li$_{0.5}$Si, we vary the occupancy of the 32 positions to control Li concentration. In structures that have higher Li content than full occupancy of the 32 positions of lowest

energy, we examine the number of Li neighbors of each Si atom and place the additional Li atoms around the Si atoms that have the lowest number of Li neighbors. The Li concentration was changed in increments of 8 Li atoms inserted (removed) at each lithiation (delithiation) step.

Due to the constraint in the in-plane directions of the unit cell, a biaxial stress is generated during lithiation and delithiation of the a-Si thin film. The evolution of the biaxial stress obtained from our first-principles calculations is shown in Figure 1. The solid-symbol line represents the stress evolution during lithiation, and the open-symbol line represents the stress during delithiation; the symbols represent the average stress of the five configurations considered at each step during lithiation and delithiation, while the error bars represent standard deviations. The agreement between the calculations and the experimental measurements is remarkable. In the calculation, during lithiation, the biaxial compressive stress reaches an elastic limit of ~2 GPa at $Li_{0.375}Si$. With further lithiation, lithiated silicon exhibits flow. The compressive flow stress decreases from ~2 to ~1 GPa when the Li composition increases to Li_2Si. Upon delithiation, lithiated silicon first unloads elastically, over a wider range of Li composition compared with the experiment. The discrepancy in the elastic unloading might be due to the creation of nanopores,[35] or to artificial limitations introduced by the relatively small size of our model system. Nevertheless, the agreement in the elastic unloading behavior between experimental measurements and theoretical predictions is still reasonable, if not as satisfactory as in the initial lithiation range. Following the elastic response, the biaxial stress reaches a value of ~1 GPa in tension, and the magnitude of the stress steadily increases with further delithiation. The high stress level at low Li concentrations might be due to an elastic response; at sufficiently low Li concentrations, the structure is too brittle to flow.[35]

We first address the question of whether or not the stress generated during the lithiation cycle is equal to the yield strength of the structure. We determine the yield strength of lithiated silicon for various Li concentrations through simulations of uniaxial tension. For each Li concentration, we first perform energy minimization of the lithiated silicon without any constraint. A given stress level is then prescribed along the x direction of the structure, and the nominal strain after full relaxation is measured. The stress−strain response curves are shown in Figure 2s (Supporting Information). More details of the simulation are described in our previous work.[35] The yield strength obtained through this procedure is shown Figure 1; the magnitude of yield strength at a fixed Li concentration is about *twice* as high as the stress generated during the lithiation cycle. The difference between the yield strength and the biaxial stress is attributed to lithiation-assisted inelastic deformation: the lithiation reaction enhances flow of lithiated silicon by lowering the stress needed to induce flow.

In order to account for these effects, we consider the following model: when an element of a Si electrode is connected to a reservoir of Li with chemical potential μ, it absorbs a number of Li ions and deforms, Figure 2a. We regard the inelastic deformation as mixing and rearranging of atoms, such that the identities of neighboring atoms are altered during deformation. The insertion of Li involves forming of Si−Li bonds and breaking of Si−Si bonds. Therefore, the lithiation-induced strain is a type of inelastic deformation. At a fixed concentration of Li, elastic deformation may also occur. It involves small changes of the relative positions of atoms but
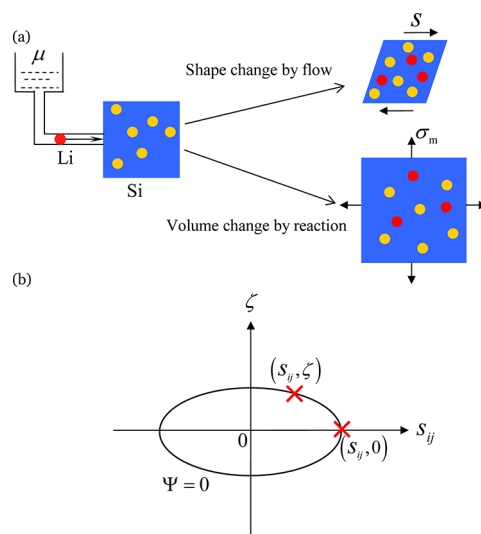
Figure 2. (a) The two types of inelastic deformation of Si during lithiation—change of shape by flow and change of volume by insertion of Li. Flow is induced by the presence of deviatoric stresses. Insertion is driven by the chemical potential μ of Li in the reservoir and the mean stress σ_m. (b) A yield function $\Psi(s_{ij}, \zeta)$ is sketched in the space of (s_{ij}, ζ); the condition $\Psi = 0$ defines the yield surface. (s_{ij}, ζ) represents the inelastic deformation driven by both the mechanical load s_{ij} and the chemomechanical load ζ, as modeled in the thin film a-Si during lithiation cycle; $(s_{ij}, 0)$ represents the inelastic deformation due only to the mechanical load s_{ij}, as modeled in the uniaxial tension simulation.

conserves the identity of neighboring atoms. The elastic deformation, typically less than 10%, is negligible compared with the large inelastic deformation caused by Li insertion. Furthermore, we distinguish two mechanisms of inelasticity of lithiated silicon——shape change by flow and volumetric change by reaction, as shown schematically in Figure 2a. Under constraints, a field of stress is induced in the electrode upon lithiation. Flow is caused by the presence of deviatoric stresses. It characterizes the shape change but conserves the volume of the electrode. This picture is reminiscent of shear flow of a metal or a liquid of small molecules. Insertion of Li induces a volume change in Si. This process is driven both by the chemical potential of Li as determined by the reservoir of Li atoms and by the mean stress generated during Li insertion; this load is referred to as the chemomechanical load. The insertion reaction and flow are concurrent during lithiation. We call the concurrent process "reactive flow". Reactive flow of solids is commonly observed in many other systems, such as oxidation of aluminum and concrete structures with alkali-silica reactions.[44−46] A full theory of reactive flow of solids is described elsewhere.[47]

Let σ_{ij} be the stress applied to the silicon electrode, $\sigma_m = (\sigma_{11} + \sigma_{22} + \sigma_{33})/3$ the mean stress, and $s_{ij} = \sigma_{ij} - \sigma_m \delta_{ij}$ the deviatoric stress, where δ_{ij} is the Kronecker delta. The chemical potential of Li in the Si electrode is $\mu_0 + kT \ln a - \Omega\sigma_m$, where μ_0 is the chemical potential of Li in the reference state, k the Boltzmann constant, T the absolute temperature, a the activity of Li in the silicon electrode, and Ω the partial molar volume of Li in Si.[20,22] A compressive mean stress retards Li insertion, and a tensile stress promotes Li insertion. When Li in the reservoir and Li in the Si electrode are not in equilibrium, the chemical potential is unbalanced. Let μ be the chemical potential of Li in the reservoir. The difference in the chemical potential between

Li in the reservoir and that in the silicon electrode defines the driving force for reaction. We write the driving force in the form

$$\zeta = \frac{\mu - \mu_0 - kT \ln a}{\Omega} + \sigma_m \tag{1}$$

When $\zeta > 0$, the imbalance in the chemical potential promotes lithiation. When $\zeta < 0$, the imbalance in the chemical potential promotes delithiation. When $\zeta = 0$, the reaction reaches equilibrium.

Following ref 47, we now regard both the reaction and flow as nonequilibrium thermodynamic processes. The driving force for reaction is ζ, and the driving force for flow is s_{ij}. Associated with ζ is the work-conjugate variable $\Omega \delta C$, which represents the volumetric response of Si upon lithiation. Associated with s_{ij} is the work-conjugate variable $\delta \varepsilon_{ij}^p$, which represents the incremental flow strain. We formulate the yield condition by placing the driving forces for reaction and flow on the same footing. Let the chemomechanical yield function be $\Psi(\mathbf{s}, \zeta)$. The condition $\Psi(\mathbf{s}, \zeta) = 0$ defines the yield surface in the linear space spanned by s_{ij} and ζ. As an example, we extend the formulation of von Mises[48] to describe reactive flow by adopting a particular form of the chemomechanical yield function:

$$\Psi = \frac{3}{2} s_{ij} s_{ij} + q \zeta^2 - \sigma_Y^2 \tag{2}$$

where σ_Y is the yield strength of lithiated silicon under uniaxial tension conditions. In general, σ_Y varies with the Li concentration and the inelastic strains, while q is a dimensionless, positive constant that indicates the relative contributions of the chemomechanical stress and the deviatoric stress to the scalar measure of the driving force for reactive flow. The value of q can be determined through a free swelling experiment, under which reactive flow due to the deviatoric stress is eliminated.

The yield surface Ψ is shown schematically in Figure 2b, represented by an ellipse in the plane spanned by (s_{ij}, ζ). We mark two important locations on the yield surface by crosses. The first point $(s_{ij}, 0)$, on the horizontal axis, represents the case of reactive flow of lithiated silicon being driven only by the mechanical force, as modeled in the uniaxial tension simulation. Under uniaxial tension, we have $s_{11} = \frac{2}{3} \sigma_Y$, $s_{22} = s_{33} = -\frac{1}{3} \sigma_Y$, and the value of the yield strength of lithiated silicon σ_Y as a function of Li concentration is taken from the results shown in Figure 1. The second point (s_{ij}, ζ) represents inelastic deformation of lithiated silicon driven by both the mechanical load s_{ij} and the chemomechanical load ζ. This situation is modeled in a thin film a-Si electrode subject to a lithiation cycle, shown in Figure 1. A biaxial stress is induced by Li insertion into a-Si thin film; under flow, $\sigma_{11} = \sigma_{22} = \tilde{\sigma}_Y$, such that $s_{11} = s_{22} = \frac{1}{3} \tilde{\sigma}_Y$, $s_{33} = -\frac{2}{3} \tilde{\sigma}_Y$. Here we differentiate between the yield strength of lithiated silicon under uniaxial tension σ_Y and the flow stress $\tilde{\sigma}_Y$ under the lithiation reaction. Their values are different, as previously mentioned (they are represented by the triangles and circles, respectively, in Figure 1). The chemomechanical driving force ζ of eq 1 can be calculated once the chemical potential of Li in the reservoir μ and the activity coefficient a are given. If we neglect the entropy contribution to the chemical potential of Li in the first-principles simulations, $\Omega \zeta$ might be represented by $-E_f$, the formation energy being defined as $E_f = E_{Li_xSi} - E_{Si} - xE_{Li}$, where

E_{Li_xSi} represents the free energy of Li_xSi, E_{Si} the free energy of the a-Si structure at the reference state, and E_{Li} the free energy of Li atoms in the bulk Li metal, taken to be the natural reservoir for Li. The particular value that ζ may assume does not affect our main findings. The important insight from this analysis, as depicted in Figures 1 and 2, is that the chemomechanical driving force can promote lithiated silicon to flow at a lower level of stresses.

The findings discussed so far concern the overall behavior of the system. In order to elucidate the origin of this behavior, we examine the atomic structures involved in the changes of mechanical behavior of Si during a lithiation cycle. We begin with the evolution of volumetric strain, shown in Figure 3a.
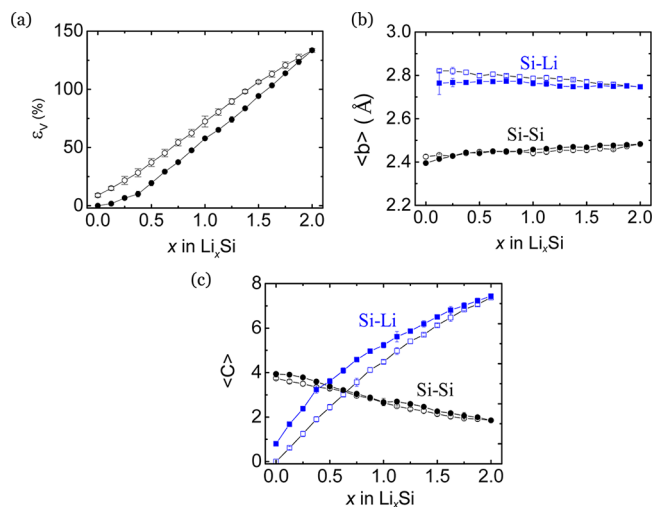
Figure 3. Structural features of an a-Si thin film during lithiation and delithiation cycle: (a) the volumetric strain, (b) the average values of Si—Si bond length and Si—Li bond length, (c) the average values of Si—Si coordination and Si—Li coordination. Solid symbol lines represent paths during lithiation, and open symbol lines represent paths during delithiation. The error bars represent standard deviations obtained from several structures at each Li concentration.

During lithiation, Si expands relatively slowly in the first stage. A large volume change takes place starting at $Li_{0.375}Si$, with the slope of the volumetric strain remaining almost constant beyond this point. At low Li concentration, Li insertion is mainly accommodated by the insertion into interstitial sites in the a-Si network. The presence of Li does not alter the Si network significantly.[32,35] Therefore, the Li insertion-induced volume change is relatively small, and the biaxial stress response is linear in the elastic regime. With further lithiation, Li insertion is accommodated by gradually rearranging the a-Si structure through Si—Si bond breaking. Li atoms have a high mobility in the a-Si network that makes it possible to induce Si—Si bond breaking and reformation, which in turn allows the system to accommodate flow of lithiated silicon, without further increase of the stress level. At the completion of a lithiation cycle, an irreversible volumetric strain of 8% is induced. We attribute this structural change to the creation of nanopores. The volume change might reach a steady state after a few cycles.[32] Figure 3b shows the evolution of Si—Si and Si—Li bond lengths that accompany these changes in volume. To define atomic bonds, a physically meaningful measure of atomic coordination is needed. We define two Si atoms to be bonded if their distance is within 10% of the covalent bond length in bulk
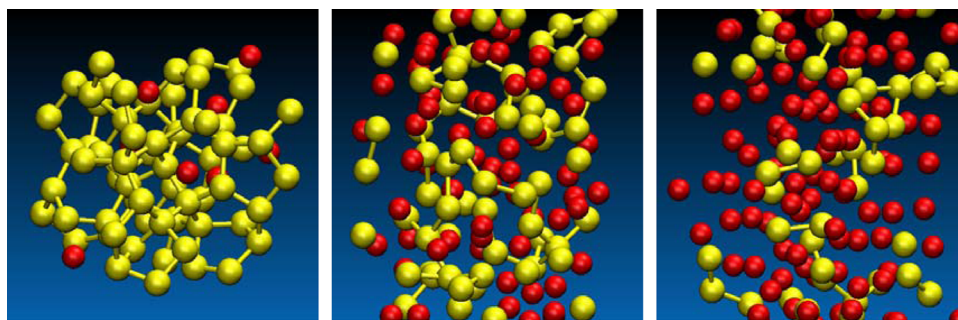
Figure 4. Examples of atomic-scale structure at different Li concentrations: $x = 0.125$ (Li$_8$Si$_{64}$, left panel), 1.0 (Li$_{64}$Si$_{64}$, central panel), and 2.0 (Li$_{128}$Si$_{64}$, right panel). Yellow spheres represent Si atoms, and red spheres represent Li atoms.

c-Si, which corresponds to the largest bond distance of 2.63 Å. We also define a Si atom to be bonded with a Li atom if their distance is smaller than 3.05 Å, a value determined by examining the distribution of Si–Li pairs in the a-Si network with the Li occupancy corresponding to the 32 unique lowest energy positions for Li atoms. Such a value is also in good agreement with calculations of molecular dynamics simulations.[49] In Figure 3b, we show the average values of the Si–Si bond length $\langle b_{Si-Si} \rangle$ and the Si–Li bond length $\langle b_{Si-Li} \rangle$. Both types of bonds remain almost constant during the lithiation cycle, with the average Si–Si bond length at ~2.45 Å and the average Si–Li bond length at ~2.78 Å. The average values of Si–Si coordination $\langle C_{Si-Si} \rangle$ and Si–Li coordination $\langle C_{Si-Li} \rangle$ as a function of Li composition are shown in Figure 3c. The atomic coordination is indicative of the deformation behavior of lithiated silicon. At low Li concentration, the Si–Si coordination changes slowly, corresponding to the elastic behavior. After Li$_{0.375}$Si, both the Si–Si coordination and the Si–Li coordination change linearly, which indicates a constant rate of Si–Si bond breaking and Si–Li bond formation. After a complete cycle of Li insertion and extraction, a fraction of Si–Si bonds, around 10%, are not recovered, representing the structural damage to the a-Si network induced by the lithiation cycle.

To illustrate the structural change mentioned so far, we show in Figure 4 three representative atomic structures at Li concentrations of $x = 0.125$ (Li$_8$Si$_{64}$), 1.0 (Li$_{64}$Si$_{64}$), and 2.0 (Li$_{128}$Si$_{64}$). In the first, with $\langle C_{Si-Si} \rangle \approx 4$, the small amount of Li present in the structure leaves the network of Si–Si bonds essentially undisturbed; in the second, with a Li:Si ratio equal to 1:1 and $\langle C_{Si-Si} \rangle \approx 3$, the network of Si–Si bonds has been significantly altered, but a fairly well-defined network of such bonds still exists and spans the size of the cell; in the third, with the Li:Si ratio equal to 2:1 $\langle C_{Si-Si} \rangle \approx 2$, the Si–Si network has been essentially destroyed and only small pockets of Si–Si bonds remain in the structure.[50,51]

Another indication of the changes to the structure upon lithiation is the overall character of the electronic properties. By analogy to studies of the crystalline-to-amorphous phase transition that occurs with the electrochemical insertion of Li into c-Si,[50,51] an improved understanding of the semiconducting-to-metallic phase transition of a-Si upon lithiation can help relate the structural properties of a-Si anodes to (macroscopically) measured electrochemical performance. In Figure 5, we show the density of states (DOS) of lithiated a-Si for a representative structure at four different concentrations of Li, $x = 0.125$ (Li$_8$Si$_{64}$), 0.25 (Li$_{16}$Si$_{64}$), 0.375 (Li$_{24}$Si$_{64}$), and 0.5 (Li$_{32}$Si$_{64}$). The corresponding DOS of the pure a-Si structure,
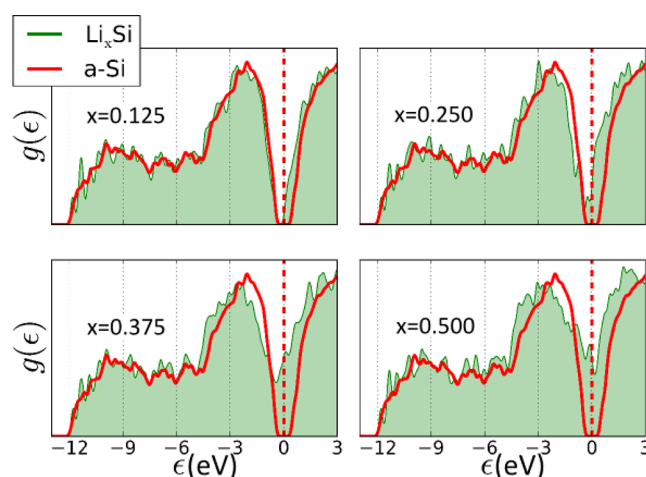
Figure 5. Density of states of pure a-Si (red solid line) and lithiated silicon (green) at Li concentrations of $x = 0.125$ (Li$_8$Si$_{64}$), 0.25 (Li$_{16}$Si$_{64}$), 0.375 (Li$_{24}$Si$_{64}$), and 0.5 (Li$_{32}$Si$_{64}$). The vertical dashed line marks the middle of the band gap or Fermi level of pure a-Si, defined as the zero of the energy scale.

which has semiconducting character with a clear gap between occupied and unoccupied states, is superimposed on each of the lithiated structures. A clear trend can be observed in these results: as the concentration of Li increases, a transition from the semiconducting to metallic phase occurs; this observation does not depend on the structure at a particular Li concentration. The main features of the transition are as follows: (i) electronic states are introduced in and around the band gap region as the band tails of a-Si broaden, a signature of bonding disorder; (ii) electronic states with energy around 2 eV below the Fermi level are depleted, which also reflects bonding distortion, since this is the energy range that characterizes Si covalent bonds; (iii) electronic states are introduced in the energy range between −5 and −2 eV that correspond predominantly to sp-states of Li. Similar observations have been reported in the work of Wan et al.[24] on the lithiation of c-Si. The semiconducting-to-metallic phase transition of a-Si during lithiation is closely correlated with the brittle-to-ductile transition behavior observed in this material.

In conclusion, we have studied the microscopic mechanism of inelastic deformation of a-Si electrodes and stresses accompanying the lithiation reaction, using first-principles calculations based on density functional theory. We described the concurrent process of the Li insertion reaction and flow of lithiated silicon. We note that reactive flow of solids is observed in many other physical systems, but its theoretical treatment is

largely undeveloped. Lithiation of silicon provides a useful model system to study the interplay of local chemical reactions and macroscopic mechanical deformation. The essence of the results in this paper is that the chemical reaction promotes mechanical flow, enabling a material to flow at a lower level of stress. We proposed a phenomenological model to describe the reactive flow of lithiated silicon and examined in detail the local atomic structures and electronic properties to elucidate the origin of the macroscopic mechanical behavior. The agreement between our theoretical treatment and experimental measurement is quite remarkable, despite the limitations of the atomistic model which come chiefly from the size of the periodic supercell to model a-Si.

Experimental Section. The Si thin-film electrode is prepared using a DC magnetron sputtering system (AJA International). A 50 nm Ti thin film was first sputtered for 5 min from a Ti target (50.8 mm diameter) onto a 175 μm thick glass substrate at 100 W power and at a pressure of 3 mTorr of argon. A 300 nm copper film was then deposited for 15 min from a Cu target (50.8 mm diameter) on the Ti underlayer at 200 W power and at a pressure of 5 mTorr of argon. The Cu film serves as the current collector, and the Ti underlayer is used to improve the adhesion between the Cu film and the glass substrate. A 100 nm Si film was subsequently deposited for 33 min from a Si target (50.8 mm diameter) at 100 W power and at a pressure of 5 mTorr of argon. All depositions were performed at room temperature. After deposition, X-ray diffraction was used to verify the amorphous structure of the Si thin film.

The Si thin film electrode was assembled in a custom three-electrode electrochemical cell (Figure 1s, Supporting Information) with pure Li as reference and counter electrodes. 1 M LiPF$_6$ in 1:1 (vol %) ethylene carbonate:diethyl carbonate was used as the electrolyte. Electrochemical measurements were performed with a VersaSTAT 3 galvanostat from Princeton Applied Research. The cell was cycled galvanostatically at a rate of 1C between 2 and 0.01 V vs Li/Li$^+$. The data acquisition rate was 1 Hz for all electrochemical measurements. The lower limit of 0.01 V was chosen to avoid formation of the crystalline Li$_{15}$Si$_4$ phase.

Stress in the silicon thin film electrode was measured by monitoring the substrate curvature during the electrochemical lithiation cycle. The average stress in the film can be deduced from the curvature of the substrate using Stoney's equation

$$\sigma = \frac{M_s h_s^2}{6 h_f} \kappa \tag{3}$$

where σ is the average stress in the film, h_s and h_f are the thicknesses of the substrate and film, respectively, k is the change in curvature of the substrate as a result of the stress, and M_s is the biaxial elastic modulus of the substrate. Note that knowledge of film properties other than film thickness is not required to calculate stresses using Stoney's equation. The film thickness h_f is taken as a function of the charge state $h_f = h_f^0(1 + 2.7m)$, where m is the state of charge and h_f^0 is the initial film thickness. This expression takes into account 370% volumetric expansion of Si upon full lithiation. Because of the constraints in the in-plane directions by the thick substrate, lithiation-induced deformation in Si is entirely accommodated by out-of-plane expansion. The curvature of the substrate was monitored with a multibeam optical sensor (MOSS) from k-Space Associates (Figure 1s, Supporting Information). The MOSS

sensor employs an array of parallel laser beams to measure the curvature of a substrate. The array of laser beams allows simultaneous multipoint illumination and detection, which in turn greatly reduces measurement noise caused by fluid motion in the electrochemical cell or by ambient vibrations. The curvature of a substrate is calculated from a geometric relation

$$\kappa = \frac{d - d_0}{2 d_0 L} \frac{n_e}{n_a} \tag{4}$$

where d is the distance between two adjacent laser spots on the CCD camera, d_0 is the initial distance between the laser spots, and L is the distance between the beaker cell and the CCD camera. Since the laser passes through the electrolyte and an optical window, refraction of the laser beams must be taken into account. In eq 4, n_e represents the refraction index of the electrolyte and n_a represents the refraction index of air. In the stress calculations, we take $n_e = 1.42$ for the electrolyte[52] and $n_a = 1.0$ for air.

■ ASSOCIATED CONTENT

Ⓢ Supporting Information

Figures showing a custom electrochemical cell with in situ multi-beam stress sensor and stress−strain responses of lithiated a-Si under uniaxial tension with different Li concentrations. This material is available free of charge via the Internet at http://pubs.acs.org.

■ AUTHOR INFORMATION

Corresponding Author
*E-mail: kaxiras@physics.harvard.edu.

Notes
The authors declare no competing financial interest.

■ ACKNOWLEDGMENTS

■ REFERENCES

(1) Zhang, W. J. *J. Power Sources* **2011**, *196* (1), 13−24.
(2) Beaulieu, L. Y.; Eberman, K. W.; Turner, R. L.; Krause, L. J.; Dahn, J. R. *Electrochem. Solid-State Lett.* **2001**, *4* (9), A137−A140.
(3) Kasavajjula, U.; Wang, C. S.; Appleby, A. J. *J. Power Sources* **2007**, *163* (2), 1003−1039.
(4) Huang, J. Y.; Zhong, L.; Wang, C. M.; Sullivan, J. P.; Xu, W.; Zhang, L. Q.; Mao, S. X.; Hudak, N. S.; Liu, X. H.; Subramanian, A.; Fan, H. Y.; Qi, L. A.; Kushima, A.; Li, J. *Science* **2010**, *330* (6010), 1515−1520.

(5) Bruce, P. G.; Freunberger, S. A.; Hardwick, L. J.; Tarascon, J. M. *Nat. Mater.* **2012**, *11* (1), 19−29.

(6) Zheng, G. Y.; Yang, Y.; Cha, J. J.; Hong, S. S.; Cui, Y. *Nano Lett.* **2011**, *11* (10), 4462−4467.

(7) Huggins, R. A.; Nix, W. D. *Ionics* **2000**, *6* (1−2), 57−63.

(8) Chan, C. K.; Peng, H. L.; Liu, G.; McIlwrath, K.; Zhang, X. F.; Huggins, R. A.; Cui, Y. *Nat. Nanotechnol.* **2008**, *3* (1), 31−35.

(9) Takamura, T.; Ohara, S.; Uehara, M.; Suzuki, J.; Sekine, K *J. Power Sources* **2004**, *129* (1), 96−100.

(10) Haftbaradaran, H.; Xiao, X.; Verbrugge, M. W.; Gao, H. *J. Power Sources* **2012**, *206*, 357−366.

(11) Yu, C.; Li, X.; Ma, T.; Rong, J.; Zhang, R.; Shaffer, J.; An, Y.; Liu, Q.; Wei, B.; Jiang, H. *Adv. Mater.* **2012**, *2* (1), 68−73.

(12) Yao, Y.; McDowell, M. T.; Ryu, I.; Wu, H.; Liu, N. A.; Hu, L. B.; Nix, W. D.; Cui, Y. *Nano Lett.* **2011**, *11* (7), 2949−2954.

(13) Hertzberg, B.; Alexeev, A.; Yushin, G. *J. Am. Chem. Soc.* **2010**, *132* (25), 8548−8549.

(14) Cui, L. F.; Hu, L. B.; Choi, J. W.; Cui, Y. *Nano Lett.* **2010**, *4* (7), 3671−3678.

(15) Wu, H.; Chan, G; Choi, J. W.; Ryu, I; Yao, Y.; McDowell, M. T.; Lee, S. W.; Jackson, A.; Yang, Y.; Hu, L.; Cui, Y. *Nat. Nanotechnol.* **2012**, *7*, 310−315.

(16) Wu, H.; Zheng, G.; Liu, N.; Carney, T. J.; Yang, Y.; Cui, Y. *Nano Lett.* **2012**, *12* (2), 904−909.

(17) Hwang, T. H.; Lee, Y. M.; Kong, B.; Seo, J.; Choi, J. W. *Nano Lett.* **2012**, *12* (2), 802−809.

(18) Sethuraman, V. A.; Chon, M. J.; Shimshak, M.; Srinivasan, V.; Guduru, P. R. *J. Power Sources* **2010**, *195* (15), 5062−5066.

(19) Li, J. C.; Dozier, A. K.; Li, Y. C.; Yang, F. Q.; Cheng, Y. T. *J. Electrochem. Soc.* **2011**, *158* (6), A689−A694.

(20) Bower, A. F.; Guduru, P. R.; Sethuraman, V. A. *J. Mech. Phys. Solids* **2011**, *59* (4), 804−828.

(21) Zhao, K. J.; Pharr, M.; Vlassak, J. J.; Suo, Z. G. *J. Appl. Phys.* **2011**, *109* (1), 016110-1−016110-3.

(22) Zhao, K. J.; Pharr, M.; Cai, S. Q.; Vlassak, J. J.; Suo, Z. G. *J. Am. Ceram. Soc.* **2011**, *94*, S226−S235.

(23) Zhao, K. J.; Pharr, M.; Wan, Q.; Wang, W. L.; Kaxiras, E.; Vlassak, J. J.; Suo, Z. G. *J. Electrochem. Soc.* **2012**, *159* (3), A238−A243.

(24) Wan, W. H.; Zhang, Q. F.; Cui, Y.; Wang, E. G. *J. Phys.: Condens. Matter* **2010**, *22* (41), 415501−9.

(25) Zhang, Q. F.; Zhang, W. X.; Wan, W. H.; Cui, Y.; Wang, E. G. *Nano Lett.* **2010**, *10* (9), 3243−3249.

(26) Zhang, Q. F.; Cui, Y.; Wang, E. G. *J. Phys. Chem. C* **2011**, *115* (19), 9376−9381.

(27) Ng, M.-F.; Sullivan, M. B.; Tong, S. W.; Wu, P. *Nano Lett.* **2011**, *11* (11), 4794−4799.

(28) Jung, S. C.; Han, Y. K. *Phys. Chem. Chem. Phys.* **2011**, *13* (48), 21282−21287.

(29) Chou, C.-Y.; Kim, H.; Hwang, G. S. *J. Phys. Chem. C* **2011**, *115* (40), 20018−20026.

(30) Kim, H.; Chou, C.-Y.; Ekerdt, J. G.; Hwang, G. S. *J. Phys. Chem. C* **2011**, *115* (5), 2514−2521.

(31) Shenoy, V. B.; Johari, P.; Qi, Y. *J. Power Sources* **2010**, *195* (19), 6825−6830.

(32) Huang, S.; Zhu, T. *J. Power Sources* **2011**, *196* (7), 3664−3668.

(33) Chevrier, V. L.; Dahn, J. R. *J. Electrochem. Soc.* **2009**, *156* (6), A454−A458.

(34) Chevrier, V. L.; Dahn, J. R. *J. Electrochem. Soc.* **2010**, *157* (4), A392−A398.

(35) Zhao, K. J.; Wang, W. L.; Gregoire, J.; Pharr, M.; Suo, Z. G.; Vlassak, J. J.; Kaxiras, E. *Nano Lett.* **2011**, *11* (7), 2962−2967.

(36) Freund, L. B.; Suresh, S. *Thin film materials*; Cambridge University Press: Cambridge, U.K., 2003.

(37) Soni, S. K.; Sheldon, B. W.; Xiao, X. C.; Tokranov, A. *Scr. Mater.* **2010**, *64* (4), 307−310.

(38) Pyun, S. I.; Go, J. Y.; Jang, T. S. *Electrochim. Acta* **2004**, *49* (25), 4477−4486.

(39) Soler, J. M.; Artacho, E.; Gale, J. D.; Garcia, A.; Junquera, J.; Ordejon, P.; Sanchez-Portal, D. *J. Phys.: Condens. Matter* **2002**, *14*

(11), 2745−2779 (we use the PBE exchange-correlation functional, norm-conserving pseudopotentials, and reciprocal-space mesh cutoff equivalent to a 10 Å real-space period for the amorphous supercell).

(40) Bazant, M. Z.; Kaxiras, E.; Justo, J. F. *Phys. Rev. B* **1997**, *56* (14), 8542−8552.

(41) Mo, Y.; Bazant, M. Z.; Kaxiras, E. *Phys. Rev. B* **2004**, *70* (20), 20510−1−205210−10.

(42) Ding, N.; Xu, J.; Yao, Y. X.; Wegner, G.; Fang, X.; Chen, C. H.; Lieberwirth, I. *Solid State Ionics* **2009**, *180* (2−3), 222−225.

(43) Xie, J.; Imanishi, N.; Zhang, T.; Hirano, A.; Takeda, Y.; Yamamoto, O. *Mater. Chem. Phys.* **2010**, *120* (2−3), 421−425.

(44) Tolpygo, V. K.; Clarke, D. R. *Acta Mater.* **2004**, *52* (17), 5129−5141.

(45) Oh, J.; Thompson, C. V. *Electrochim. Acta* **2011**, *56* (11), 4044−4051.

(46) Ulm, F. J.; Coussy, O.; Li, K. F.; Larive, C. *J. Eng. Mech. Div., Am. Soc. Civ. Eng.* **2000**, *126* (3), 233−242.

(47) Brassart, L.; Suo, Z. G. *J. Mech. Phys. Solids* **2012**, submitted for publication.

(48) Hill, R. *The Mathematical Theory of Plasticity*; Oxford University Press: Oxford, U.K., 1950.

(49) Cui, Z. W.; Gao, F.; Cui, Z. H.; Qu, J. M. *J. Power Sources* **2012**, *207*, 150−159.

(50) Key, B.; Bhattacharyya, R.; Morcrette, M.; Seznec, V.; Tarascon, J.-M.; Grey, C. P. *J. Am. Chem. Soc.* **2009**, *131* (26), 9239−9249.

(51) Johari, P.; Qi, Y.; Shenoy, V. B. *Nano Lett.* **2011**, *11* (12), 5494−5500.

(52) McAuthur, M. A. An in-situ investigation of solid electrolyte interphase formation on electrode materials for lithium-ion batteries using spectroscopic ellipsometry. Thesis for the Degree of Master of Science, Dalhousie University, 2011.